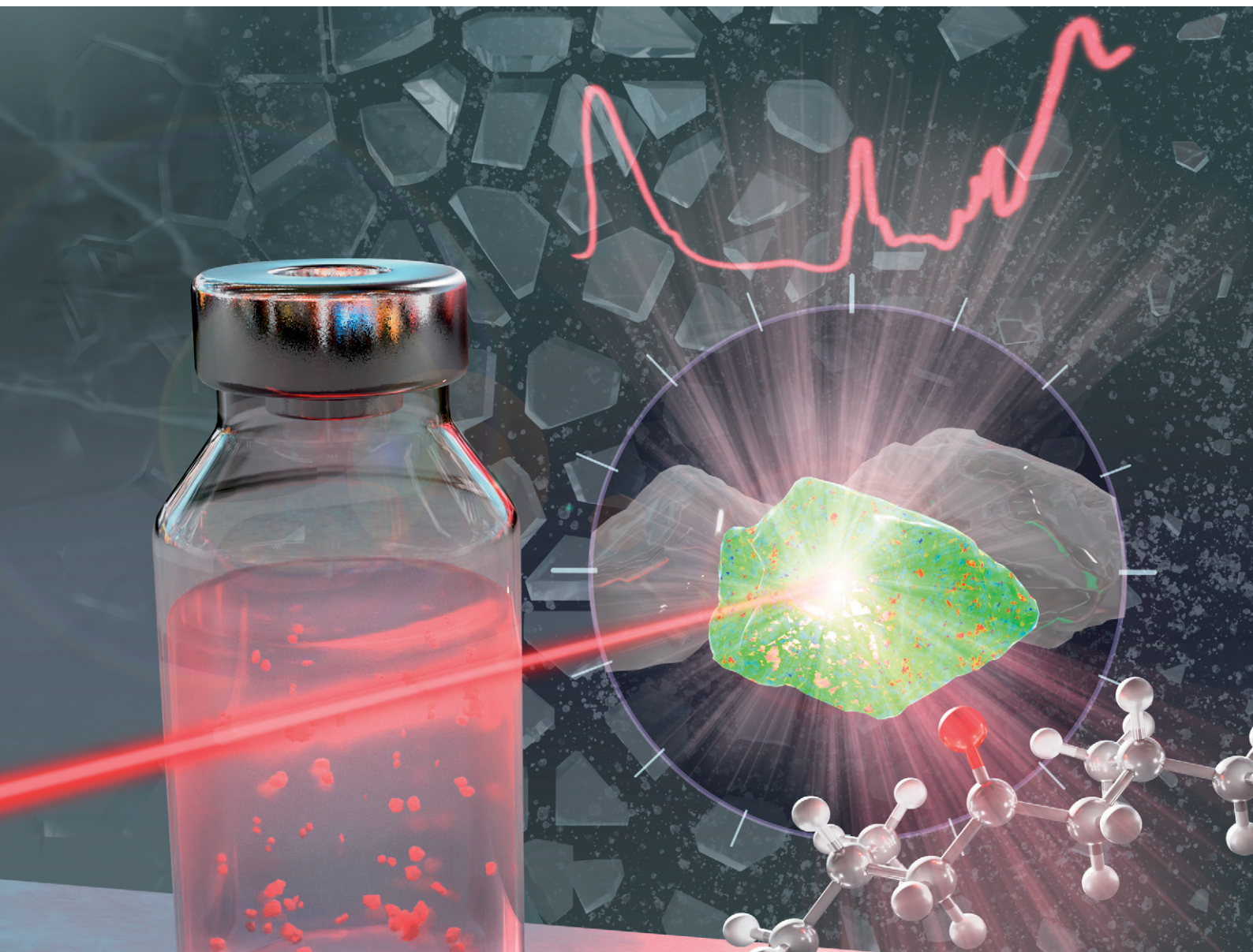


# Environmental Science Nano

Volume 13  
Number 3  
March 2026  
Pages 1237-1742

rsc.li/es-nano



ISSN 2051-8153

#### PAPER

Andrea Mario Giovannozzi *et al.*

Multiparameter characterisation of a nano-polypropylene representative test material with fractionation, light scattering, high-resolution microscopy, spectroscopy, and spectrometry method



Cite this: *Environ. Sci.: Nano*, 2026, 13, 1391

# Multiparameter characterisation of a nano-polypropylene representative test material with fractionation, light scattering, high-resolution microscopy, spectroscopy, and spectrometry methods

Dorota Bartczak, <sup>a</sup> Aneta Sikora, <sup>a</sup> Heidi Goenaga-Infante, <sup>a</sup> Korinna Altmann, <sup>b</sup> Roland Drexel, <sup>c</sup> Florian Meier, <sup>c</sup> Enrica Alasonati, <sup>d</sup> Marc Lelong, <sup>d</sup> Florence Cado, <sup>d</sup> Carine Chivas-Joly, <sup>d</sup> Marta Fadda, <sup>e</sup> Alessio Sacco, <sup>e</sup> Andrea Mario Rossi, <sup>e</sup> Daniel Pröfrock, <sup>f</sup> Dominik Wippermann, <sup>f</sup> Francesco Barbero, <sup>g</sup> Ivana Fenoglio, <sup>g</sup> Andy M. Booth, <sup>h</sup> Lisbet Sørensen, <sup>h</sup> Amaia Igartua, <sup>h</sup> Charlotte Wouters, <sup>i</sup> Jan Mast, <sup>i</sup> Marta Barbaresi, <sup>j</sup> Francesca Rossi, <sup>k</sup> Maurizio Piergiovanni, <sup>j</sup> Monica Mattarozzi, <sup>j</sup> Maria Careri, <sup>j</sup> Thierry Caeberts, <sup>l</sup> Anne-Sophie Piette, <sup>l</sup> Jeremie Parot <sup>m</sup> and Andrea Mario Giovannozzi <sup>l</sup> \*<sup>e</sup>

Reference and quality control materials with comparable physicochemical properties to nanoplastic contaminants present in environmental and food nanoplastics are currently lacking. Here we report a nanoplastic polypropylene material prepared using a top-down approach involving mechanical fragmentation of larger plastics. The material was found to be homogeneous and stable in suspension and has been characterised for average particle size, size distribution range, particle number concentration, polypropylene mass fraction and inorganic impurity content using a wide range of analytical methods, including AF4, cFFF, PTA, (MA)DLS, MALS, SEM, AFM, TEM, STEM, EDS, Raman, ICP-MS and pyGC-MS. The material was found to have a broad size distribution, ranging from 50 nm to over 200 nm, with the average particle size value dependent on the technique used to determine it. Particle number concentration ranged from 1.7–2.4 × 10<sup>10</sup> g<sup>-1</sup>, according to PTA. Spectroscopy techniques confirmed that the material was polypropylene, with evidence of aging due to an increased level of oxidation. The measured mass fraction was found to depend on the marker used and ranged between 3 and 5 µg g<sup>-1</sup>. Inorganic impurities such as Si, Al, Mg, K, Na, S, Fe, Cl and Ca were also identified at ng g<sup>-1</sup> levels. Comparability and complementarity across the measurement methods and techniques is also discussed.

Received 30th September 2025,  
Accepted 23rd December 2025

DOI: 10.1039/d5en00917k

rs.li/es-nano

## Environmental significance

Reliable reference and quality control materials are essential for advancing nanoplastics research, yet materials with properties comparable to those found in environmental and food samples remain scarce. In this work, we present a polypropylene nanoplastic material produced through mechanical fragmentation, providing a representative and well-characterised model for environmental contaminants. The material shows stability in suspension and has been comprehensively characterised for particle size, concentration, composition, and impurities using a wide range of state-of-the-art analytical methods. By offering a realistic, traceable, and versatile test material, this study supports improved method validation, comparability across laboratories, and more robust risk assessment of nanoplastics in environmental and food contexts.

<sup>a</sup> National Measurement Laboratory, LGC Limited, 10 Priesley Road, Guildford, UG2 7XY, UK

<sup>b</sup> Bundesanstalt für Materialforschung und –prüfung (BAM), Unter den Eichen, 87, Berlin, Germany

<sup>c</sup> Postnova Analytics GmbH, Rankinestr. 1, 86899 Landsberg a. Lech, Germany

<sup>d</sup> Laboratoire National de Métrologie et d'Essais (LNE), 1 rue Gaston Boissier, 75015 Paris, France

<sup>e</sup> Istituto Nazionale di Ricerca Metrologica (INRiM), Strada delle Cacce 91, 10135 Torino, Italy. E-mail: a.giovannozzi@inrim.it

<sup>f</sup> Institute of Coastal Environmental Chemistry, Inorganic Environmental Chemistry, Helmholtz-Zentrum Hereon, Max-Planck Str. 1, 21502 Geesthacht, Germany

<sup>g</sup> Department of Chemistry, University of Torino, Torino, Italy

<sup>h</sup> Department of Climate and Environment, SINTEF Ocean, Trondheim, Norway

<sup>i</sup> Trace Elements and Nanomaterials, Sciensano, Groeselenberg 99, 1180 Uccle, Belgium

<sup>j</sup> Department of Chemistry, Life Sciences and Environmental Sustainability, University of Parma, Parco Area delle Scienze 17/A, 43124 Parma, Italy

<sup>k</sup> IMEM, CNR Institute of Materials for Electronics and Magnetism, Parco Area delle Scienze 37/A, Parma, 43124, Italy

<sup>l</sup> DG Quality and Safety, Metrology Division (SMD), FPS Economy, Bd du Roi Albert II, 16, 1000 Brussels, Belgium

<sup>m</sup> Department of Biotechnology and Nanomedicine, SINTEF Industry, Trondheim, Norway



# 1. Introduction

Over 350 million tons of plastic waste are produced globally every year, of which nearly two-thirds are estimated to be released into the environment as plastic waste.<sup>1</sup> Numerous international organisations, including the United Nations (UN), World Health Organization (WHO), and Organisation for Economic Co-operation and Development (OECD), have called for action to increase our understanding and to propose effective mitigation measures to protect the public and the environment from plastic pollution. In Europe, the European Commission (EC) has responded through policy documents, including the green deal and the EU plastics strategy. The EC has also advanced legislation, including the registration, evaluation, authorisation, and restriction of chemicals (REACH) and the drinking water directive (DWD, 2020/2184 (ref. 2)). In the United Kingdom, the government has set a target of eliminating avoidable plastic waste by the end of 2042 to prevent further pollution with plastics.

Despite joint international efforts to reduce the amount of plastic waste, it continues to be released into the environment at an unprecedented scale.<sup>3</sup> Once in the environment, plastics undergo fragmentation upon exposure to UV radiation and through mechanical stress.<sup>4</sup> Larger pieces of plastic are fragmented into microplastics (MPs), defined as particles in the size range from 1  $\mu\text{m}$  to 1  $\text{mm}$ <sup>5</sup> or 5  $\text{mm}$ ,<sup>6</sup> and eventually to nanoplastics (NPs), with sizes below 1000  $\text{nm}$ .<sup>7</sup> MPs and NPs have been reported in all environmental compartments, accumulating in soils and sediments, and considered critical persistent pollutants of increasing global concern owing to their high durability and long-life.<sup>8</sup>

The potential long-term impacts on biota and human health arising from MPs and NPs present in the environment are still unknown, and there are no defined maximum daily exposure limits due to the lack of robust toxicological data.<sup>9</sup> This is, in part, due to the absence of metrologically validated, harmonised and standardised measurement methods, as well as the lack of consensus with regard to the typical quantities (per size class, especially for particles with sizes below 1000  $\text{nm}$ ) and physicochemical characteristics of various types of plastics typically occurring in the environment. There remains a need to develop robust analytical methods for plastic characterisation, especially at the sub-micron and nanoscale.

The characterisation and quantification of plastic particles <1000  $\text{nm}$  is challenging due to their multimodal and polydisperse character and irregular shape, but also due to the limitations of analytical techniques routinely used for the characterisation of other types of particles in the size range from 1–1000  $\text{nm}$ . For instance, commonly used light scattering techniques, such as dynamic light scattering ('DLS' or multi-angle DLS 'MADLS'<sup>10</sup>), multi-angle static light scattering (MALS<sup>11</sup>) or particle tracking analysis (PTA<sup>12</sup>), as well as high-resolution microscopy methods, such as transmission electron microscopy (TEM<sup>13</sup>), scanning electron

microscopy (SEM<sup>14</sup>) or atomic force microscopy (AFM<sup>15</sup>) are compatible with particles in that size range, but they cannot easily distinguish between plastic particles and other types of particles that might also be present in the sample.<sup>16</sup> Conversely, spectrometry-based methods, such as pyrolysis gas chromatography-mass spectrometry (pyGC-MS), can distinguish plastic particles but do not provide information about particle size or morphology.<sup>16</sup> Moreover, most of the imaging spectroscopy methods, such as micro-Raman ( $\mu\text{Raman}$ ) or micro-Fourier transform infrared spectroscopy ( $\mu\text{FTIR}$ ), have size detection limits >1000  $\text{nm}$  and are therefore unable to characterise and quantify particles in the nanoscale.<sup>17</sup>

These limitations with individual techniques highlight the need for the development of alternative multi-technique, hyphenated (*e.g.* multidetector field-flow fractionation 'FFF'<sup>16</sup>) or hybrid approaches (*e.g.* SEM/RAMAN,<sup>18</sup> dielectrophoresis (DEP)-Raman<sup>19,20</sup>) involving a combination of measurement methods, allowing simultaneous characterisation of multiple parameters at the nanoscale, including chemical identity, particle size, and size distribution, as well as mass and number concentration. Such combined approaches will be invaluable in supporting policymakers, international standardisation efforts and testing laboratories, and will enable the development and characterisation of future NP quality control (QC) measures and reference materials (RMs), which are currently unavailable.

This work describes a systematic evaluation of the applicability of selected light scattering, fractionation, high-resolution microscopy, spectroscopy and spectrometry methods, as standalone techniques and in combination (including hyphenated and hybrid), for characterising plastic particles <1000  $\text{nm}$ . Assessment was conducted using a combination of commercially available polystyrene (PS) microspheres and more environmentally relevant polypropylene (PP) nanoplastic particles produced through a top-down method. The complementarity and comparability of the different analysis techniques are discussed, including when applied in combination, along with main sources of measurement errors for selected techniques and measurands.

## 2. Experimental section

### 2.1. Materials

**2.1.1. Monodispersed polystyrene spheres.** A single batch of PS microspheres of approximately 200  $\text{nm}$  ( $202 \pm 4 \text{ nm}$ ),  $k = 2$  (Duke 3200A) was purchased from Thermo Fisher (Fremont, CA) to use as a quality control material (QC). The material was characterised by the manufacturer for size using TEM and was supplied with indicative information on the solid content. In addition, 60  $\text{nm}$  PS beads with a certified size ( $60 \text{ nm} \pm 4 \text{ nm}$ , Nanosphere™ Size Standard 3060A) were purchased from Thermo Fisher Scientific (Waltham, MA, USA).



**2.1.2. Polydispersed polypropylene particles.** A polydispersed nanoPP test material containing particles <1000 nm in size was produced by fragmenting PP pellets with an UltraTurrax and subsequently applying filtration (Fig. 1), as described elsewhere.<sup>21</sup> Approximately 25 g of PP pellets were placed into a glass beaker containing 250 mL acetone. The beaker was pre-cooled on ice (0 °C) for 30 min and crushed for 10 min with 18000 rpm after which the suspension was filtered through a pleated filter (Labsolute Partikelret. 5–8 µm, 100% cellulose) to remove larger particles. The particles on the filter were washed twice with 20 mL acetone. The volume of the resulting filtrate was then reduced to 10% (*ca.* 25 mL) by rotary evaporation (temperature water bath: 55 °C, pressure 510–530 mbar), before adding 250 mL of ultrapure water. The suspension was subjected to rotary evaporation again to remove the remaining acetone by reducing the pressure. After reaching a pressure of 100 mbar the conditions remain constant for another 30 min. Temperature of the water bath: 55 °C. The resulting aqueous suspension was filtered again *via* a clean, but similar, pleated filter. The final filtrate was divided into 890 brown glass vials, each containing ~2 mL of PP suspension. The procedure described by Hildebrandt *et al.*<sup>21</sup> was repeated by BAM approximately 60 times, using ~6 g starting material. For the purpose of the work described here the amount of starting material was increased from 6 g to 25 g, however the resulting particles show comparable characteristics in terms of particle size distribution to the material described by Hildebrandt *et al.*<sup>21</sup>

Since the candidate reference material and representative test materials are typically prepared as a single batch which is then portioned into multiple vials/containers, the homogeneity and stability of such materials are typically assessed based on between unit variability, as described in

ISO 33405:2024. The homogeneity of the nanoPP material was investigated by analysing the content of 15 units in duplicate by PTA to determine particle size and number concentration (as described in section 2.2). Material stability was tested periodically using batch DLS analysis (as described in section 2.2) at time 0, 1 month, 3 months and 6 months, covering the period over which all measurements described in the work reported here were performed. Three bottles were measured in duplicate at each time point. All materials were diluted, as required by each technique, in ultrapure water (18.2 MΩ cm, 25 °C, Elga Purelab Chorus, Viola Water Technologies, Buckinghamshire, UK) prior to analysis, unless stated otherwise.

## 2.2. Instruments and methods

**2.2.1. PTA.** A NanoSight NS300 (PTA; Malvern Panalytical Ltd., UK) system equipped with a laser module with a wavelength at 405 nm, a high sensitivity scientific complementary metal-oxide-semiconductor (sCMOS) camera, a syringe pump and low-volume-flow-cell (LVFC) was used by Postnova Analytics and LGC. UNITO used a ZetaView® PMX-120 PTA (Particle Metrix GmbH, Germany), equipped with a light source with a wavelength of 488 nm and a 90° laser scattering video microscope with 10× magnification. The instruments were switched on 30 min prior to measurement. The flow-through cells were cleaned with ultrapure water before each new sample injection, as well as between individual aliquots of the same sample and at the end of all measurements, until no more particles are detected. For the NanoSight NS300, each sample was diluted gravimetrically ~100× in ultrapure water to a final particle number concentration of approximately 20–100 particles per frame and shaken manually prior to analysis. Measurements

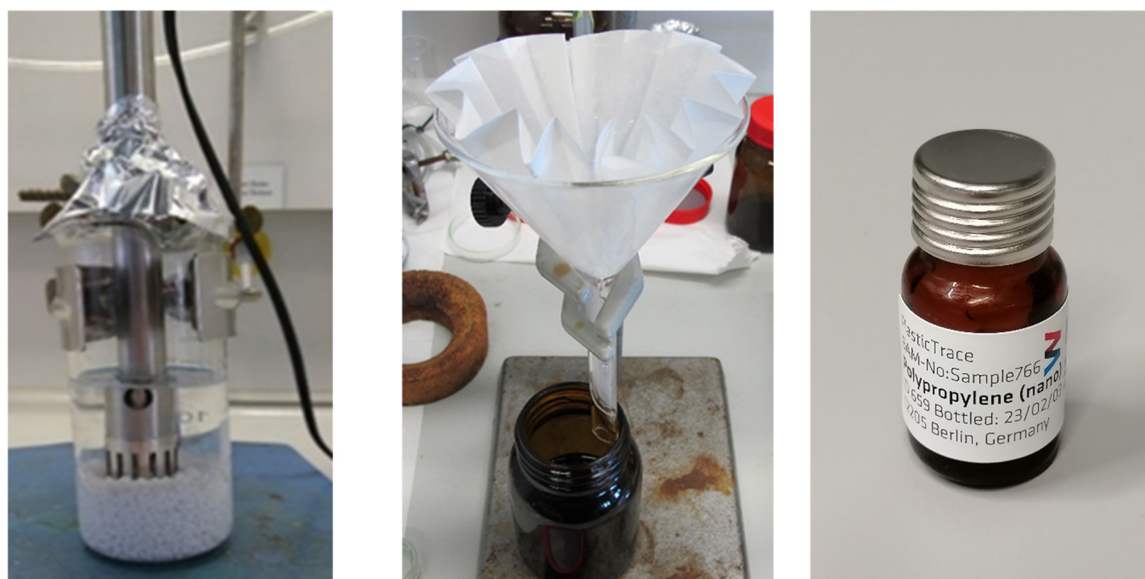


**Fig. 1** Fragmentation of PP pellets with UltraTurrax (left), filtration of fragmented PP for fractionation (centre) and the final bottled PP suspension (right).<sup>21</sup>



were performed in a flow mode, and the camera settings and focus were optimised manually. All measurements were conducted at room temperature, allowing the instruments to automatically determine the actual temperature in the flow cell and assign an associated water viscosity value for data analysis. Captures with a duration of 60 s were recorded and repeated 5 times per sample. For analysis by PMX-120, each sample was diluted  $\sim 700$  times (gravimetrically). The sensitivity and shutter were set to 80 and 100, respectively, with a frame rate of 30 fps and a minimum track length of 15 frames. For each sample, 3 sets of 33 videos (1 second each) were recorded, analysing a minimum of  $\sim 2500$  NPs per measurement.

**2.2.2. DLS (MADLS).** A MADLS Zetasizer Ultra instrument (Malvern Panalytica, UK) equipped with  $173^\circ$ ,  $90^\circ$  and  $13^\circ$  angles and a low-volume, high-performance black quartz cuvette (ZEN 2112) was used by LGC and INRIM. The MADLS instruments were switched on at least 30 min prior to analysis. At LGC, the sample was analysed both undiluted and following an  $\sim 10\times$  dilution in ultrapure water. Individual samples were measured 3–5 times under the following repeatability conditions: analysis temperature  $25^\circ\text{C}$ , with media viscosity set to  $0.8872\text{ mPa s}$  and the refractive index (RI) set to 1.33, while the material RI was set to 1.49 and the absorbance set to 0.01. Multiple narrow peak mode was used. At INRIM, 5 runs per measurement were conducted on each undiluted sample. The operating temperature was maintained at  $25^\circ\text{C}$ . The average hydrodynamic diameter ( $z$ -average) and polydispersity index (PDI) were obtained from the correlation function fitted according to ISO 22412:2017.

**2.2.3. FFF-MALS.** At Hereon, centrifugal FFF (cFFF) measurements were performed using a CF2000 system (Postnova Analytics, Landsberg a. L., Germany) equipped with an autosampler, a degasser unit and a UVD disinfection unit. The system was equipped with an analytical fractionation channel with a thickness of  $231\ \mu\text{m}$ , a channel area of  $100\text{ cm}^2$  and a void volume of  $2\text{ mL}$ . A typical injection volume of  $20\ \mu\text{L}$  was used for the measurements. The method employed a start speed of  $3500\text{ rpm}$  and maintained a flow rate of  $1.5\text{ mL min}^{-1}$ . The injection time was set to 38 seconds, followed by a relaxation time of 5 min. The carrier liquid was  $0.2\%$  (v/v) NovaChem100. The cFFF system was connected to a MALS detector (PN3621). After each run, a rinse step of 10 min was conducted to overcome potential carry over effects and ensure reproducible conditions for subsequent measurements. At the end of measuring each batch of samples, a blank run was performed injecting only MilliQ. In total, 3 samples with 4 replicates each were fractionated and characterised. Samples were diluted five-fold in MilliQ prior to analysis. Evaluation of the data obtained from the MALS detector was conducted by applying a sphere model to the scattering data. Typically, the range of  $12^\circ$  to  $156^\circ$  was used for data evaluation, where  $68^\circ$  and  $132^\circ$  were excluded from evaluation as these angles did not provide

sufficient data owing to the detectors needing to be replaced.

At Postnova Analytics, multi-detector (MD)-AF4 experiments were performed on an AF2000 MT system (Postnova Analytics, Landsberg a. L., Germany). An analytical AF4 channel with a tip-to-tip length of  $277\text{ mm}$ , a width of  $20\text{ mm}$  and a hip width of  $5\text{ mm}$  was equipped with a regenerated cellulose membrane (RC) with a molecular weight cut-off of  $10\text{ kDa}$  and a  $350\ \mu\text{m}$  spacer height. The temperature during fractionation was kept constant at  $25^\circ\text{C}$  using a channel thermostat. The samples were injected using an autosampler. The fractionation system was directly coupled to a UV/Vis detector and a MALS detector (21 active angles, laser wavelength  $532\text{ nm}$ ). The UV absorbance was measured at  $254\text{ nm}$ . The MALS detector was normalised using fractionated  $60\text{ nm}$  PS beads and a spherical fit model. A volume of  $20\ \mu\text{L}$  of a  $40\text{ ppb}$  nanoPP suspension was injected as received, with no sample preparation performed. The carrier liquid consisted of  $0.2\%$  (v/v) NovaChem100 (PN). For the fractionation, a detector flow rate of  $0.50\text{ mL min}^{-1}$ , an injection flow rate of  $0.20\text{ mL min}^{-1}$  and an injection time of 5 min were applied. The initial cross flow rate was set to  $1.20\text{ mL min}^{-1}$ . After a transition time of 0.2 min, the cross-flow rate was kept constant for 0.2 min and then decreased within 40 min using a power decay (exponent = 0.2) to  $0.10\text{ mL min}^{-1}$ . This last cross flow rate was kept for 10 min, followed by a rinse step of 5 min. All measurements were conducted in duplicate. In total, 12 vials (each with 2 aliquots) were fractionated and characterised. MALS data evaluation was performed within an angular range of  $12^\circ$  to  $156^\circ$ , and the scattering intensities were evaluated by fitting a sphere model to the angular dependent scattering data to obtain size information (radius of gyration,  $R_g$ ). This type of fit model yielded results with low deviations across the complete size range with squared correlation coefficients above 0.98. The sphere model represented the data points accurately around the peak maximum. Slight deviations for the smallest and largest size fractions were observed, but comparable results were derived from a fourth order polynomial fit. The system was controlled by the NovaFFF Software (version 2.2.0.1) and data evaluation was performed in the NovaAnalysis software (version 2408).

At LNE, MD-AF4 analysis was performed on an AF4 system (AF2000 Postnova Analytics) coupled to MALS (DAWN HELEOS II, Wyatt Technology) equipped with 18 angles and UV (SPD-20A, Shimadzu) detectors. A metal-free analytical AF4 channel (tip-to-tip length of  $277\text{ mm}$ ,  $20\text{ mm}$  width and  $5\text{ mm}$  hip width) (Postnova Analytics) was used. The carrier liquid was prepared by dissolving Novachem100 (Postnova Analytics) in ASTM type I ultrapure water to a final concentration of  $0.0125\%$  and passing through a  $0.1\ \mu\text{m}$  filter (RC, Postnova Analytics). The channel out-let flow rate was  $0.5\text{ mL min}^{-1}$ . MALS data treatment was performed using the Berry model of second degree, 11 angles and the Astra Software (version 6.1.7, Wyatt Technology). The UV detector was used for MALS data treatment and for recovery



calculation. The uncertainty associated with the  $R_g$  was established as the combination of the repeatability, the average MALS model uncertainty and the size bias between the certified value and the measured value of a 200 nm PS standard. Blanks consisting of pure carrier liquid were injected between samples and no carry over was observed. Aliquots of the nanoPP suspension were characterised without any dilution or further sample treatment (e.g. filtration or ultrasonication).

At SMD, MD-AF4 analysis was performed on a Wyatt Eclipse DualTec, equipped with a UV/Vis detector (Agilent G7114A), a MALS detector (DAWN HELEOS II, Wyatt Technology), and an inline Malvern Zetasizer Nano ZS (Malvern Panalytical, UK). The carrier was SDS (0.01% m/v) in ultrapure water, filtered through a 0.1  $\mu\text{m}$  filter (RC, Millipore). The separation method was an isocratic program for most of its duration and separation. The UV/Vis wavelength was set to 200 nm, and blank subtraction applied.

**2.2.4. TEM and STEM-EDX.** At Sciensano, conventional TEM imaging was performed using a Tecnai G2 Spirit 12 (120 kV, Thermo Fisher Scientific, Eindhoven, The Netherlands) with BioTwin lens configuration equipped with a 4X4K Eagle CCD camera and using TIA software (Thermo Fisher Scientific). In addition, a Talos F200S G2 (200kV, Thermo Fisher Scientific) equipped with a Ceta 16 M camera, high angle annular dark field (HAADF) detector, Super-X detector and Velox software (Version 3.8, Thermo fisher scientific) was used for scanning TEM coupled with energy dispersive x-ray spectroscopy (STEM-EDX) to perform chemical mapping. The 200 nm PS QC material was diluted 10 times using MilliQ water and deposited on Alcian blue pre-treated pioloform- and carbon-coated copper grids (Agar Scientific, Essex, England) by grid-on-drop deposition (10' contact).<sup>22</sup> The size properties of the particles were measured semi-automatically from TEM images using the ParticleSizer plugin<sup>23</sup> in the ImageJ software. The total measurement uncertainty was determined by a validation study, following an approach similar to Verleysen *et al.*,<sup>24</sup> consisting of three replicate measurements per day for 5 consecutive days and measuring at least 500 particles per measurement (see detailed methodology in SI, section E). The nanoPP suspension was used undiluted and different methods for the TEM grid preparation were tested: untreated, Alcian blue pre-treated and glow discharged pioloform- and carbon-coated copper grids (Agar Scientific, Essex, England). Sample deposition on the grid was done by either grid-on-drop deposition (10' contact), drop-on-grid deposition followed by evaporation drying<sup>22</sup> (overnight), or on-grid ultracentrifugation. Size properties of particles were measured manually from TEM images in ImageJ.

At the University of Parma, TEM analysis was performed using a JEOL JEM-2200FS field-emission microscope equipped with an EDX detector (Oxford Xplore), operated at an accelerating voltage of 200 kV.<sup>25,26</sup> Ultra-thin carbon-coated copper grids (200 mesh, Electron Microscopy Society)

were selected to provide optimal support. The images were recorded in both TEM imaging mode using a Gatan UltraScan US1000 camera and in STEM imaging mode using a HAADF detector. For each grid, 20 micrographs were acquired in random sampling mode, ensuring coverage of both the border and centre regions of the grid. Ultrapure water blanks were analysed to detect any potential contamination introduced during sample preparation and handling. Particle counting and sizing were performed using the open-source ImageJ software. The intensity range was adjusted to isolate particles from the background. To improve particle separation and minimise noise, manual thresholding and morphological filtering were applied. Sample preparation was performed in a cleanroom (ISO level 6) to minimise cross-contamination. Glassware was pre-cleaned according to the internal standard operating procedure developed within the PlasticTrace project, involving a sequential washing and sonication for at least 5 minutes using TritonX-100 (0.1 mg L<sup>-1</sup>), acetone and an isopropanol/water solution (20% v/v). A suspension of the 200 nm PS QC material was diluted in ultrapure water to a final concentration of 0.04 mg mL<sup>-1</sup>. A 20  $\mu\text{L}$  aliquot of the suspension was then drop-cast on the TEM grid and dried at room temperature. Three different sample preparation protocols were tested using nanoPP suspensions at a nominal concentration of 0.04 mg mL<sup>-1</sup>. (i) Drop-casting: an aliquot of 100  $\mu\text{L}$  of the nanoPP suspension was dried in a clean vial at 50 °C, reconstituted with 30  $\mu\text{L}$  of ultrapure water, dried again, and reconstituted with an additional 10  $\mu\text{L}$  of ultrapure water. The final suspension was then drop-cast on the TEM grid and dried at room temperature. (ii) Concentration by heating bath: 100  $\mu\text{L}$  of the nanoPP suspension was placed directly into a vial containing the TEM grid and dried at 50 °C using a hot bath. Subsequently, the sample was reconstituted with 30  $\mu\text{L}$  of ultrapure water directly over the grid and dried again. (iii) Concentration by SpeedVac, drying and drop-casting: 2 mL of the nanoPP suspension was dried at 50 °C using a SpeedVac system. The sample was reconstituted with 30  $\mu\text{L}$  of ultrapure water, dried again, and reconstituted with an additional 10  $\mu\text{L}$  of ultrapure water. The final suspension was then drop-cast on a TEM grid and dried at room temperature.

**2.2.5. SEM.** SEM analysis was conducted using a Zeiss ultra-plus SEM with a field emission source and a gemini column. The in-lens detector measured secondary electrons at 3 kV at a 3.0 mm working distance. A charge compensator system was used to blow nitrogen gas near the samples and neutralise negative charges. Samples were prepared using conventional evaporation deposition, where an aliquot of the nanoPP suspension was placed directly onto the silicon support. For each sample, three series of 300 particles were counted and measured using the Platypus software developed by Pollen Metrology,<sup>27</sup> allowing the type-A uncertainty related to repeatability of the SEM measurements to be determined. The estimation of the statistic law parameters that best fitted the SEM data for each sample was carried out using R-Studio



software with a program developed by the LNE statistics team.<sup>28</sup> The size distributions measured by EM-based analysis were fitted by a log-normal function. The output mean diameter ( $d_{eq. mean}$ ) and standard deviation ( $s$ ) were determined, associated with the 95%-confidence interval for both parameters.

**2.2.6. AFM.** AFM measurements were performed with an Asylum Research MFP-3D Infinity instrument, operated in intermittent contact mode. Olympus AC160 and Nanosensors PPP-NCHR tips were selected depending on the substrate and to optimise the imaging. The instrument was calibrated against step height topography standards for Z-scale (height) measurements, which are the most accurate as they are less affected by the tip convolution effect compared to lateral size measurements.

**2.2.7. DEP-RAMAN and SEM/RAMAN.** At INRiM, Raman spectra of 10 vials of nanoPP were acquired by coupling DEP and Raman spectroscopy. A 50  $\mu\text{L}$  aliquot of each suspension was mixed with 5  $\mu\text{L}$  of 10% PBS solution, after which, a 5  $\mu\text{L}$  aliquot was injected into a home-made DEP cell. The electrical field in the DEP cell was induced by a sinusoidal voltage of 5 V peak-to-peak at a frequency of 1 MHz obtained by a Hewlett-Packard 33120a (United States) function generator. This resulted in negative DEP and net forces on the samples directed towards the centre of the cell, where the confocal volume of a Raman Imaging microscope (DXRxi, Thermo Scientific, United States) was located. The accumulation time before Raman spectra acquisition was 30 s. Spectra were acquired with a 60 $\times$  water immersion objective (N.A. = 1.1) using an excitation wavelength at 532 nm, a laser power of 20 mW, an exposure time of 1 s for 60 scans (1 minute total per spectrum), and a spectrograph confocal pinhole aperture of 50  $\mu\text{m}$  in diameter. The dispersive Raman system has 5  $\text{cm}^{-1}$  spectral resolution and a spectral range of 500–3100  $\text{cm}^{-1}$ .

At LNE, a drop of the nanoPP suspension was deposited on a silicon wafer and identified by using  $\mu\text{Raman}$  (LabRAM Soleil<sup>TM</sup> Confocal Raman Microscope) equipped with LabSpec 6 software. Raman spectra were acquired using a 532 nm laser at 50% power, with a 200  $\mu\text{m}$  aperture and a 600 lines per mm grating (500 nm). The exposure time was set to 1 s with 10 accumulations. Measurements were performed using a 100 $\times$  objective over a spectral range of 500–3500  $\text{cm}^{-1}$ . The resulting spectra were compared with the IDFinder spectral library for particle identification.

**2.2.8. pyGC-MS.** Six replicate aqueous nanoPP suspension samples were individually homogenised by gentle shaking followed by 250  $\mu\text{L}$  from each bottle being sub-sampled into pyrolysis cups for quantification. MilliQ water was used as blank samples. The water was removed by gentle evaporation prior to analysis. Pyrolysis gas chromatography-mass spectrometry (PyGC-MS) was performed using a Frontier Multi-Shot Pyrolyzer (PY-3030D) coupled to an Agilent 7890A GC with an Agilent 5975C MS (Py-GC/MS) (Santa Clara, CA, USA). The pyrolyzer was operated in single-shot mode with pyrolysis at 600  $^{\circ}\text{C}$  (1.0 min). The pyrolyzer interface and GC

inlet temperatures were 320  $^{\circ}\text{C}$ , and the split ratio was 25:1. The carrier gas was helium at a constant flow of 1  $\text{mL min}^{-1}$ . Separation was achieved using a Frontier Ultra ALLOY+5 capillary column (30 m length, 0.25  $\mu\text{m}$  film thickness, and 0.25 mm internal diameter). The column oven temperature was programmed at 40  $^{\circ}\text{C}$  (2 min) and ramped up by 20  $^{\circ}\text{C min}^{-1}$  until it reached 320  $^{\circ}\text{C}$  (25 min hold). The transfer line temperature was 320  $^{\circ}\text{C}$ , the ion source temperature was 230  $^{\circ}\text{C}$ , and the quadrupole temperature was 150  $^{\circ}\text{C}$ . The ion source was operated in SIM mode using several established target peaks for quantification of PP: 2,4-dimethylhept-1-ene using marker ions  $m/z$  70 and 126; 2,4,6-trimethyl-1-nonene (meso) and 2,4,6-trimethyl-1-nonene (racemic) using marker ions  $m/z$  69 and 97; 2,4,6,8-tetramethyl-1-undecene (isotactic), 2,4,6,8-tetramethyl-1-undecene (heterotactic) and 2,4,6,8-tetramethyl-1-undecene (syntactic) using marker ions  $m/z$  69 and 111. External calibration curves were prepared from an in-house standard PP reference material by complete solvent dissolution and subsequent dilution to different concentrations. For calibration, a standard PP powder (PP Co-polymer CRT201.00 from CARAT GmbH, <100  $\mu\text{m}$ ) was dissolved in xylene (130  $^{\circ}\text{C}$ , 30 min followed by ultrasonication in a sonication bath, 10 min 80  $^{\circ}\text{C}$ ), diluted and spiked in resulting masses of 0.25–5  $\mu\text{g}$  in stainless steel pyrolysis cups. Samples were run in randomised order, with triplicate calibration samples run throughout the series, also in randomised order. It is important to note that the PP powder used for calibration was not produced from the same PP pellets used to generate the nanoPP test material (section 2.1.2).

**2.2.9. ICP-MS/MS and AF4/MALS/ICP-MS.** At Hereon, triplicate samples of 50  $\mu\text{L}$  ( $n = 2$ ) and 500  $\mu\text{L}$  ( $n = 1$ ) were digested using 5 mL  $\text{HNO}_3$ , 2 mL  $\text{HCl}$  and 1 mL  $\text{HBF}_4$ . Samples were digested at 220  $^{\circ}\text{C}$  and 48 bar using microwave assisted acid digestion (BLADE microwave, CEM Corp., Kamp Lintfort, Germany). TFM digestion vessels were pre-cleaned using an ETC EVO II (ANALAB, Hoenheim, France) acid vapor cleaner with  $\text{HNO}_3$  (65% w/w) and type I reagent grade water. Digested samples were quantitatively transferred to 50 mL graduated, PP vessels (DigitUBE<sup>®</sup>; SCP Science, Quebec, Canada) pre-cleaned with  $\text{HNO}_3$  (2% w/w) and filled to a total volume of 50 mL with type I reagent grade water. Sample digests were measured using an ICP-MS/MS (Agilent 8800, Agilent Technologies, Santa Barbara CA, USA) coupled to a prepFAST M5 system (Elemental Scientific, Omaha, Nebraska, USA). A special inert sample introduction kit (AHF analysentechnik AG, Tübingen, Germany) was used to minimise the responses in the blank samples.  $\text{H}_2$  and  $\text{N}_2\text{O}$  were employed as reaction gases in MS/MS mode for the quantified elements. Quantified mass-to-charge ratios and corresponding cell modes were selected based on achieved sensitivity, as well as by non-occurrence of isobaric and polyatomic interferences. The instrument was tuned daily to obtain optimal measuring conditions using a tune solution containing Li, Co, Y, Ce and Tl (10  $\mu\text{g L}^{-1}$ ). External calibration covering a concentration range from 0  $\mu\text{g L}^{-1}$  to



10 000  $\mu\text{g L}^{-1}$  for Si, P, Mg, Al, K, Ca, Ti and Mn automatically diluted by the prepFAST M5 system from two stock solutions (500  $\mu\text{g L}^{-1}$  and 10 000  $\mu\text{g L}^{-1}$ ), as well as online dosed internal standards (10  $\mu\text{g L}^{-1}$  Rh and Ir) were used for quantification. Potential carry-over effects were monitored by measuring wash blanks (2%  $\text{HNO}_3$  (w/w)) after each triplicate of samples. Calibration solutions were freshly prepared immediately before measurement.

At Postnova, AF4/MALS/ICP-MS measurements were performed using an AF4 system, as described under 2.2.3, that was hyphenated to ICP-MS (7900 ICP-MS, Agilent Technologies Inc. USA). The hyphenation was realised using an ICP-MS module (PN 9040), which connected the MALS detector outlet with a T-piece connected to the ICP-MS. Sample introduction on the ICP-MS system consisted of a MicroMist nebuliser and a concentric Scott spray chamber. A plasma gas flow rate of 15  $\text{L min}^{-1}$  and a nebuliser gas flow rate of 1.05  $\text{L min}^{-1}$  were applied. All measurements were conducted at a maximum radio frequency power of 1550 W. A collision gas of 4.5  $\text{mL min}^{-1}$  of helium was introduced into the collision cell to remove potential polyatomic interferences. The ICP-MS performance was checked and tuned prior to the measurements. The isotopes  $^{24}\text{Al}$ ,  $^{27}\text{Al}$ ,  $^{28}\text{Si}$ ,  $^{31}\text{P}$ ,  $^{35}\text{Cl}$ ,  $^{38}\text{Ca}$ ,  $^{47}\text{Ti}$ ,  $^{52}\text{Cr}$ ,  $^{56}\text{Fe}$ ,  $^{60}\text{Ni}$ ,  $^{63}\text{Cu}$ ,  $^{66}\text{Zn}$ ,  $^{79}\text{Br}$ , and  $^{90}\text{Zr}$  were monitored with an integration time of 0.1 s. The carrier liquid consisted of 0.0125% (v/v) NovaChem100 and the same fractionation method was used as described under 2.2.3. The injection volume was increased to 100  $\mu\text{L}$ . A 200 nm PS bead with a maximum injection amount of 4  $\mu\text{g}$  was used as a control.

## 3. Results and discussion

### 3.1. Homogeneity and stability

Most polypropylene particles present as contaminants in food and the environment arise from the packaging materials, mainly food packaging. All food contact materials are designed to contain minimum amount of other additives, which is the reason why a material characterised in the work reported here has been design to contain predominantly particles composed of pure polymer and yet is considered to resemble in terms of its properties nanoplastic contaminants. The material was prepared using a top-down method<sup>21</sup> that mimics the mechanical fragmentation process and results in polydispersed in shape and size particles that exhibit signs of ageing (*i.e.* oxidation at the surface).

This material, like majority of other reference materials and representative test materials, was prepared as a single batch, which was then portioned into multiple vials/containers. The homogeneity and stability of this material were hence assessed based on between unit variability, as described in ISO 33405:2024. The PTA technique was chosen for the purpose of the nanoPP material's homogeneity assessment as it allows determination of hydrodynamic size and particle number concentration independent from each other, which are considered critical measurands for particles

at the sub-micron and nanoscale. For particle size, the modal particle size was evaluated. The size was less variable than particle number concentration, with no clear outliers detected for either of the two measurands. For the modal particle size, uncertainty associated with homogeneity was around 4.4%. In the case of particle number concentration, this value was around 14.4%.

The material's stability was tested using DLS, since this light technique is more sensitive to the presence of agglomerates/aggregates (a strong indicator of particle instability) than number-based methods such as PTA. DLS provides information on particle size and size distribution. No significant differences in particle size and particle size distribution were observed over a 6-month period.

### 3.2. Characterisation of nanoPP

**3.2.1. Particle size and size distribution.** The particle size and size distribution of nanoPP were measured in solution with number-based instrumentation (PTA), ensemble intensity-based instrumentation (DLS and MADLS) and ensemble size-resolved instrumentation (MD-AF4), as well as following deposition on solid supports (SEM, AFM and TEM). Results from the PTA analyses are presented in Fig. 2 and Table 1 as average mean size values with associated standard deviation. In addition, LGC also calculated the associated measurement uncertainty.

As can be seen in Fig. 2 (black line), the size distribution of the particles in the nanoPP material determined by the NanoSight NS300 instruments suggests a polydisperse distribution with multiple modes and broad size distribution tailing towards larger sizes. This is consistent with a material produced *via* a top-down approach using mechanical fragmentation and sieving to increase the environmental relevance. The size distribution for the PMX-120 instrument (red line) is shifted towards larger sizes, which might be related to effects arising from the data processing algorithms the two different instruments use. Due to the multimodal and polydispersed character of the nanoPP material, the mean particle size rather than the modal particle size is considered the most appropriate and more practical measurand for the purpose of comparison with intensity-based methods (like DLS) described in the following sections. Even in this case, the mean particle size value measured by the PMX-120 instrument is slightly larger (170.4 nm) than the values determined by the NanoSight NS300 instruments (147.0 and 148.1 nm). However, if expanded measurement uncertainty ( $k = 2$ ), calculated as being  $\sim 10$ – $11\%$  according to Eurachem/CITAC guidelines, is considered for the purpose of data comparison, the results obtained across all three instruments are in agreement within the associated measurement uncertainty. Measurement repeatability was identified as being the main factor ( $\sim 50\%$  of the uncertainty budget) contributing to the overall uncertainty, as expected for a polydisperse material. The size obtained for the PS QC material was  $201.4 \pm 2.9$  nm (LGC),  $195.4 \pm 2.2$  nm (Postnova)



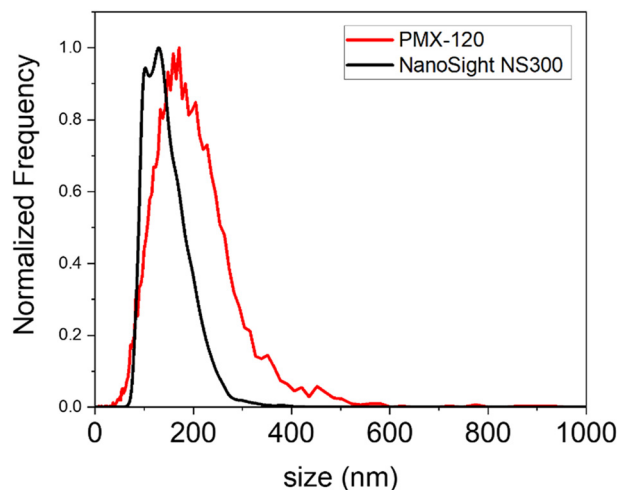


Fig. 2 Average size distribution graphs obtained with PTA using NanoSight NS300 (black line) and PMX-120 (red line).

Table 1 Particle mean size obtained with PTA

Institute	Instrument	nanoPP particle mean size (nm)		
		Average (nm)	Stdev (nm)	RSD (%)
LGC	NanoSight NS300	148.1 ( $n = 45$ )	5.5 ( $n = 45$ )	4.0
Postnova	NanoSight NS300	147.0 ( $n = 24$ )	3.5 ( $n = 24$ )	2.4
UNITO	PMX-120	170.4 ( $n = 15$ )	4.4 ( $n = 15$ )	2.6

and  $204.4 \pm 1.5$  nm (UNITO), in agreement with the size value reported by the manufacturer ( $202 \pm 4.0$  nm) and consistent across all experimental set-ups tested.

The particle size and size distribution of the nanoPP suspension were also measured with MADLS by LGC and batch DLS by INRIM. The results are presented in Table 2 as average mean size values (MADLS) or average hydrodynamic diameter (z-average; DLS), with associated standard deviation of  $n$  measurements. Mean particle size was similar for both DLS ( $174.9 \pm 0.4$  nm) and MADLS ( $186.0 \pm 3.9$  nm), with the slight difference between the two values suggested to be a result of data processing algorithms, being the cumulants method in the case of DLS and the distribution algorithm, or so called ‘multiple narrow mode’, for MADLS. The cumulants model assumes a single particle population, which is represented as a simple Gaussian distribution, with the z-average being the mean size value. In contrast, the distribution algorithm models the correlogram as an intensity contribution for each size band/bin. As such, the cumulants model for a material exhibiting a polydisperse non-Gaussian distribution, as in the case of the nanoPP material, might give different results than MADLS. As both DLS and MADLS are intensity-based methods, they are more sensitive to the presence of larger particles than number-based methods such as PTA, which results in the slightly larger mean particle size for the former.

The results obtained by the different FFF-based methodologies are summarised in Table 3. The AF4-MALS

Table 2 Particle mean or z-average size obtained with MADLS and DLS, respectively

Institute	Particle mean or z-average size (nm)		
	Average (nm)	Stdev (nm)	RSD (%)
LGC (MADLS)	186.0 ( $n = 41$ )	3.9 ( $n = 41$ )	2.1
INRIM (DLS)	174.9 ( $n = 15$ )	0.4 ( $n = 15$ )	0.2

measurements performed by Postnova on the nanoPP suspension showed excellent repeatability, with a mean retention time of  $26.71 \pm 0.34$  min ( $n = 24$ ) (Fig. 3). The peak width and peak shape across all investigated aliquots were very comparable, with insignificant field-off and void peaks. The average MALS  $90^\circ$  signal across all measurements is displayed in black, and the grey area visualises the standard deviation of the MALS  $90^\circ$  signals. As the retention time is directly proportional to the particle hydrodynamic size, the size can be derived using FFF theory. The derived weight-average  $R_{g,w}$  of  $75.0$  nm  $\pm$   $0.9$  nm (mean  $\pm$  stdev,  $n = 48$ ) is equivalent to a sphere with a diameter of 194 nm. The mean particle size derived from angular dependent MALS signal intensities yielded an  $R_{g,50} = 74.2$  nm  $\pm$   $0.8$  nm (mean  $\pm$  stdev,  $n = 48$ ), which is equivalent to a geometrical sphere with a diameter of 191 nm. Both values are in good agreement with FFF theory and PTA and DLS results.

At LNE, six replicates of each nanoPP vial were analysed on two different days to include daily variability in the measurement precision. The results of the characterisation show excellent repeatability (Table 3), but the  $R_g$  values obtained using MALS were slightly larger than obtained on the different instrumental set-up at Postnova. Nonetheless, if measurement uncertainties ( $k = 1$ ) are considered, the results are in agreement within the associated errors. They also agree with PTA and MADLS data. It is also important to mention that channel recoveries of  $> 70\%$  were obtained using the AF4-based method (meeting method acceptance criteria described in ISO 21362 (ref. 29)). Similar results were obtained at SMD (Table 3 and SI, section E). At Hereon, 4 replicates of each nanoPP vial were analysed using cFFF coupled to MALS.  $R_g$  values obtained with this instrumental set-up were in agreement with values reported for AF4 (see SI, section F, for details). It is also important to mention that channel recoveries of  $> 70\%$  were obtained at all labs and with all systems, meeting method acceptance criteria described in ISO 21362.<sup>29</sup>

SEM-EDX was used to obtain size and size distribution data on nanoPP, as well as elemental information. Representative SEM images shown in Fig. 4 reveal that the nanoPP material comprised particles with irregular shapes and a broad size distribution, ranging from  $\sim 50$  nm to  $\sim 160$  nm and a modal size of  $\sim 93.9$  nm (with standard measurement uncertainty  $k = 1$  of 2.3 nm). The EDX spectrum of the imaged particle population in the nanoPP sample revealed clearly visible peaks relating to the oxygen O Ka line (Fig. 5). The observable S Ka signal potentially comes



**Table 3** Summary of the size values obtained using the FFF method, with their associated uncertainties ( $u$ ,  $k = 1$ ), and recovery values. Radii of gyration and hydrodynamic radii, respectively, are displayed as number ( $R_n$ ), weight ( $R_w$ ) and z-averages ( $R_z$ ). Additionally, cumulative radii values at 50% are listed in the table as  $R_{50}$  values

Institute	Set-up	Radius	$R_n$		$R_w$		$R_z$		$R_{50}$		System recovery (%)
			Mean $\pm$ stdev <sup>a</sup> (nm)	$u$ , $k = 1$ (%)	Mean $\pm$ stdev <sup>a</sup> (nm)	$u$ , $k = 1$ (%)	Mean $\pm$ stdev <sup>a</sup> (nm)	$u$ , $k = 1$ (%)	Mean $\pm$ stdev <sup>a</sup> (nm)	$u$ , $k = 1$ (%)	
Postnova	AF4-MALS 90° signal	Hydrodynamic			102.5 $\pm$ 2.1	2.0			98.2 $\pm$ 1.7	1.7	>75
Postnova	AF4-MALS	Gyration - sphere	46.3 $\pm$ 3.8	8.2	75 $\pm$ 0.9	1.2	96.3 $\pm$ 3.6	3.7	74 $\pm$ 0.8	1	>75
LNE	AF4-UV-MALS	Gyration	81 $\pm$ 4 <sup>a</sup>	5	86 $\pm$ 4 <sup>a</sup>	5	91 $\pm$ 5 <sup>a</sup>	6	—	—	~74
SMD	AF4-UV-MALS	Gyration -	64 $\pm$ 10	16	92 $\pm$ 3	3	111 $\pm$ 2	1	—	—	> 70
Hereon	cFFF-MALS	Gyration -	65 $\pm$ 5	8	67 $\pm$ 5	7	69 $\pm$ 5	7	—	—	> 70

<sup>a</sup>  $n$  (number of replicate measurements) is given in the Experimental, Results and/or SI sections.

from the isotactic form of the PP polymer, with cross linkage in the presence of sulphur.<sup>30</sup> The copper peak Cu La and the carbon peak C Ka come from the substrate (carbon and pioloform coated Cu grid) used to deposit the particles, whilst the Al Ka signal comes from the sample holder.

STEM-EDX analysis of the nanoPP material, deposited by various methods, revealed the presence of several chemical compounds (mostly salts and other inorganic compounds, see SI, section F). The particles are suspended in water. Even if MilliQ water was used, it seems reasonable to assume that the salts originated from the PP raw material or the material processing to derive the nanoPP suspension, rather than the water dispersant itself. Grids prepared by grid-on-drop deposition and using Alcian blue grid staining resulted in the least amount of interference of various deposited compounds. From such a grid, a size histogram of area-equivalent circular diameter (ECD) was constructed based on the manual measurement of 74 particles, resulting in a mean ECD of 166 nm (SI, section F, Fig. 1), consistent with the results from characterisation techniques able to analyse the

particles in suspension. The limited statistics reflect the low particle concentration on the grid. While most particles were isolated, a few agglomerates were also observed, in which case constituent particles that could be resolved visually were measured individually. The composition of a subset of particles was verified by STEM-EDX to be sure that the C signal, indicative of plastic composition, was dominating. However, since C is also present in the supporting film, it cannot be said with certainty that the particles included in the size analysis are nanoPP.

SI, section E, gives an overview on how to validate TEM for reliable determination of particle size and shape based on the 200 nm PS QC material. It demonstrates that accurate and precise measurements can be obtained for monomodal and monodispersed nanoplastic particles, when the particle concentration is sufficiently high. In contrast, attempts to measure the size of nanoPP demonstrate that detection and analysis of environmentally relevant nanoplastics with TEM is much more challenging. Currently, there is no reliable method to selectively separate and enrich nanoplastics with low abundancies to enable analysis in the same way as QC materials. While analytical TEM, such as STEM-EDX, can be useful for detecting false-positive plastic identifications through elemental composition analysis and thus serve as a complementary technique to DLS and PTA, it cannot directly confirm the presence of plastics. Analysis of the nanoPP material by STEM-EDX at the University of Parma TEM produced results that were in agreement with those described above (see SI, section G).

With (classical) AFM performed at SMD only mechanical measurement was possible. Reliable dimensional measurement was achieved by using the deposition method described in the Results section, which yielded a sufficient amount of particles without visible agglomeration. Overall, the size range measured with AFM was in agreement with the size reported by SEM and TEM (see SI, section H for details).

The results of nanoPP size characterisation with the techniques described above are summarised in Fig. 6, where blue markers highlight techniques providing hydrodynamic diameter, yellow markers represent techniques providing

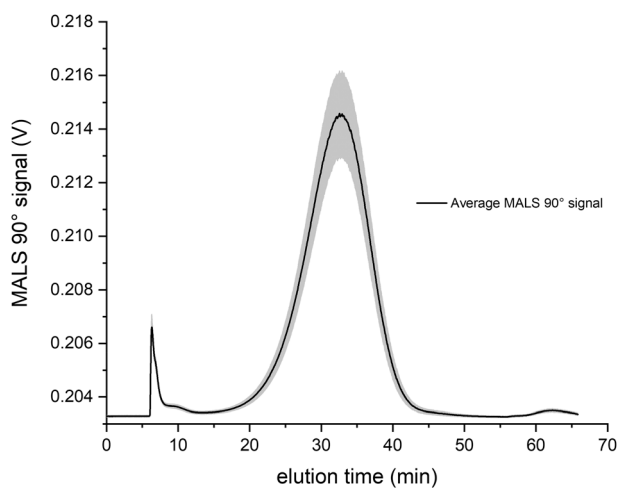


**Fig. 3** Average AF4-MALS elution fractogram obtained with 90° angle by Postnova.



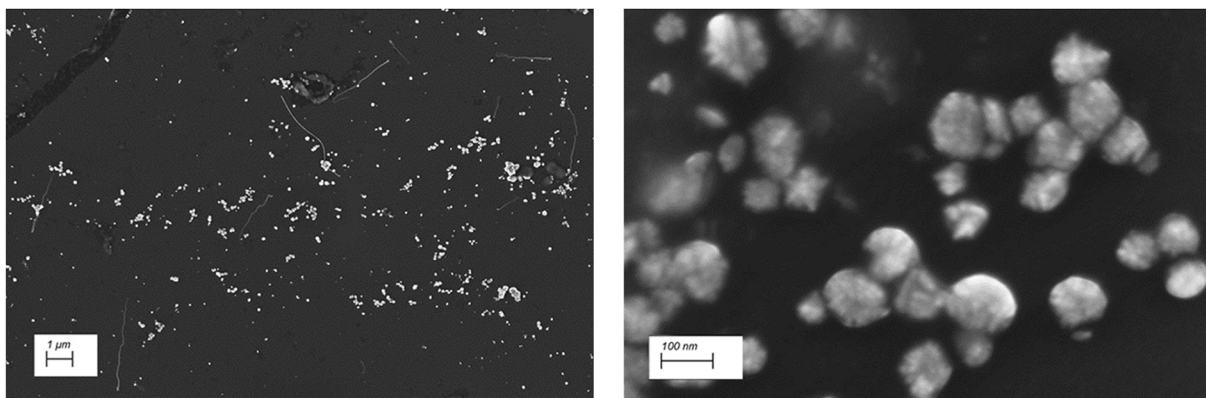


Fig. 4 Representative SEM images of particles present in the nano-PP sample with magnification  $\times 10\,000$  for the image on the left and magnification  $\times 100\,000$  for the image on the right.

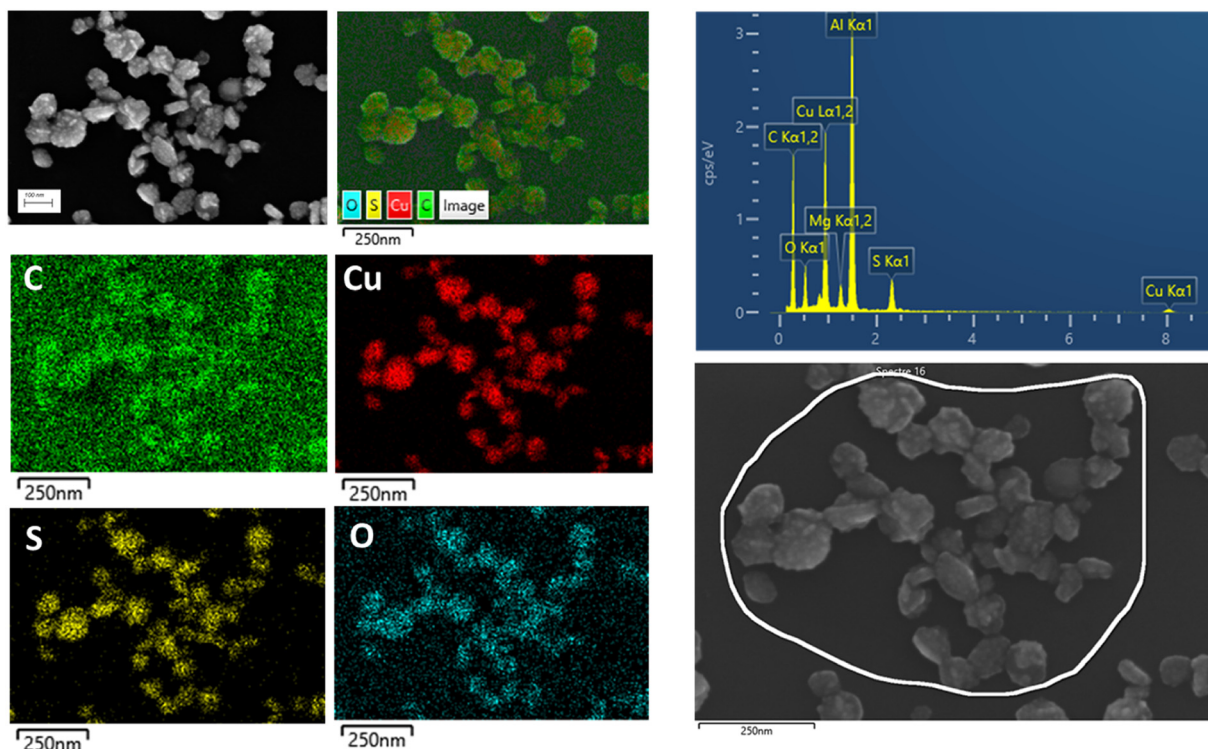
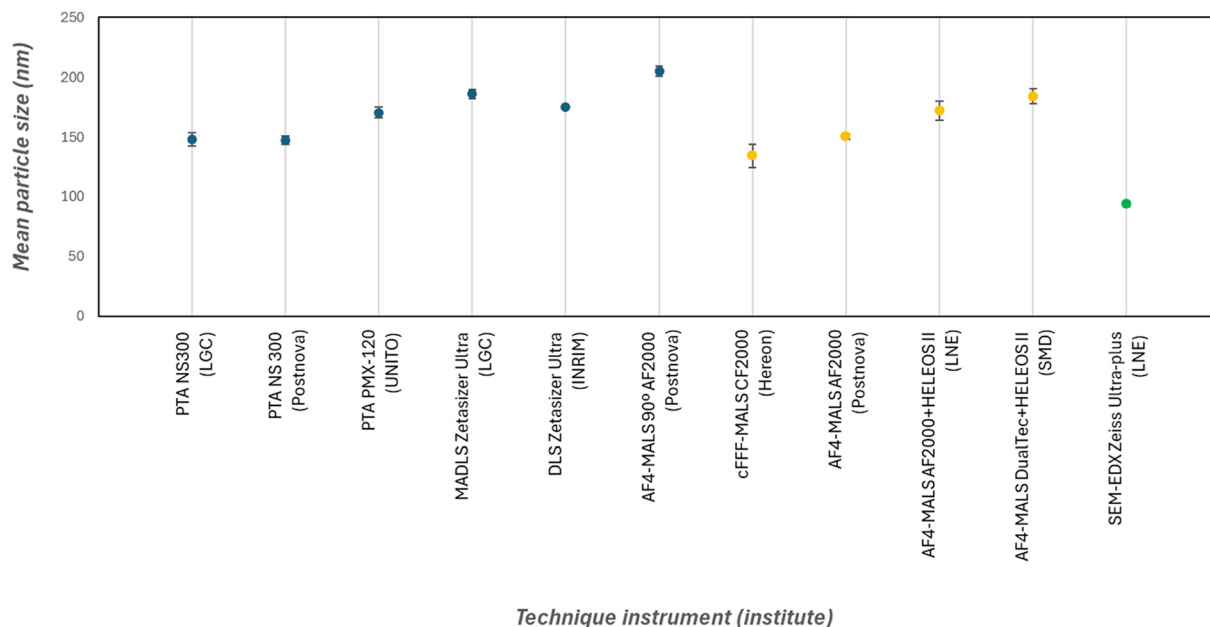


Fig. 5 EDX spectrum obtained for the selection of particles present in the nanoPP sample as indicated on the SEM image (right) and EDX mapping in the same area (left).

geometric size, whilst a green marker is an equivalent modal size from the surface area (obtained *via* SEM), which all represent different measurands (although all size related) and hence cannot be compared like-for-like. Typically, hydrodynamic diameter is larger than geometric size, which in turn is larger than equivalent size obtained from electron microscopy techniques representing the particle core only, and not accounting for a hydration layer or surface bound ligands or stabilisers. Furthermore, whilst AF4, CF3, DLS/MADLS and PTA results represent mean particle size, SEM results show modal particle size, which for polydispersed particles with non-Gaussian tailing distribution can indeed be larger. In the case of PTA (LGC results) the same data

sets with a mean particle size of  $148.1 \pm 5.5$  nm (average  $\pm$  stdev,  $n = 45$ ) would give a modal particle size value of  $118.2 \pm 15.1$  nm (average  $\pm$  stdev,  $n = 45$ ), being much closer to the SEM result. Another point to consider is weighting of the results, whilst PTA and SEM represent number-weighted particle size, DLS and MADLS are intensity weighted, hence predominantly influenced by the presence of larger particles, resulting in larger size, especially for polydispersed materials, like nanoPP. It is also important to mention that the difference in size reported here between techniques could also be additionally exaggerated by between lab variability, which was not studied as part of the work reported here.





**Fig. 6** Summary of nanoPP size characterisation. Data points represent average size whilst scale bars represent standard deviation of these measurements. Blue markers highlight techniques providing hydrodynamic diameter, markers in yellow represent techniques providing geometric size, whilst a green marker is an equivalent modal size from surface area.

**3.2.2. Particle number concentration.** Particle number concentration, expressed as the number of particles per mass of the neat nanopolypropylene suspension (*i.e.*  $\text{g}^{-1}$ ), as recommended in ISO TS 24672 documentary standard, was measured with PTA by LGC and Postnova (using NS300 instruments) and UNITO (using a PMX-120 instrument), with the results presented as average particle number concentrations with associated standard deviation (Table 4). In addition, LGC also calculated the associated measurement uncertainty as being  $\sim 19\%$  ( $k = 2$ , calculated according to Eurachem/CITAC guidelines), with repeatability in particle counting identified as the main contributing factor ( $\sim 80\%$ ). The nanoPP concentrations determined across the 3 instruments range from  $1.73 \times 10^{10} \pm 2.47 \times 10^9$  to  $2.4 \times 10^{10} \pm 2.6 \times 10^9$ , which are in agreement, considering the associated measurement uncertainty ( $k = 2$ ).

**3.2.3. Chemical identification.** In Fig. 7 Raman spectra are shown for bulk PP (as reference; grey), nanoPP with DEP off (red, background), and nanoPP with DEP on (blue). All nanoPP peak assignments are highlighted and detailed in the SI (section I), alongside a comparison to the bulk PP. The observed spectral changes in the nanoPP Raman spectrum can be attributed to a combination of mechanical fragmentation, solvent-induced swelling/extraction, and oxidative aging processes during preparation. It is already known that the production process influences the surface properties of the particles and causes oxidized functional groups, as described elsewhere.<sup>31</sup> The shift of the symmetric  $\text{CH}_2$  stretching peak from  $2840 \text{ cm}^{-1}$  to  $2848 \text{ cm}^{-1}$  likely reflects altered chain packing and conformational strain in the nanosized particles, where reduced crystallinity and increased surface-to-volume ratio modify vibrational

environments, as commonly seen in top-down nanoplastic production involving cryogenic milling or solvent-assisted grinding.<sup>21,31–34</sup> New carbonyl ( $\text{C}=\text{O}$ ) peaks at  $1650 \text{ cm}^{-1}$  and  $1605 \text{ cm}^{-1}$  indicate partial oxidation of the PP surface, facilitated by acetone's role as a swelling agent that exposes amorphous regions to atmospheric oxygen, with shear forces from Ultraturrax accelerating reactive species formation (*e.g.*, peroxides leading to ketones/carboxylic acids).<sup>33,34</sup> In the fingerprint region, shifts such as  $1436 \rightarrow 1445 \text{ cm}^{-1}$  ( $\text{CH}_2$  bending),  $1254 \rightarrow 1277 \text{ cm}^{-1}$  ( $\text{CH}_3$  rocking), and others ( $1219 \rightarrow 1202$ ,  $1168 \rightarrow 1157$ ,  $1153 \rightarrow 1127$ ,  $940 \rightarrow 929 \text{ cm}^{-1}$ ) arise from lattice contraction and amorphization upon nanosizing, reducing peak resolution and intensities while eliminating crystalline-sensitive bands at  $842 \text{ cm}^{-1}$  and  $810 \text{ cm}^{-1}$  (replaced by a broader  $830 \text{ cm}^{-1}$  feature). These modifications confirm nanoPP's chemical identity as oxidized polypropylene, with differences stemming from preparation-induced aging rather than phase transformation (Fig. 7).<sup>19</sup>

Correlative SEM/Raman analysis was also performed on a drop of the nanoPP suspension deposited on a silicon wafer to assess the global chemistry. As chemical analysis of individual nano-scale particles by Raman is not possible due to the limited size resolution of this technique in the nanometer size regime, bulk analysis can be used to generate

**Table 4** Particle number concentration obtained with PTA

Institute	Particle number concentration ( $\text{g}^{-1}$ )		
	Average ( $\text{g}^{-1}$ )	Stdev ( $\text{g}^{-1}$ )	RSD (%)
Postnova	$1.73 \times 10^{10}$ ( $n = 24$ )	$2.47 \times 10^9$ ( $n = 24$ )	14.3
LGC	$2.04 \times 10^{10}$ ( $n = 45$ )	$1.78 \times 10^9$ ( $n = 45$ )	8.7
UNITO	$2.4 \times 10^{10}$ ( $n = 15$ )	$2.6 \times 10^9$ ( $n = 15$ )	10.8



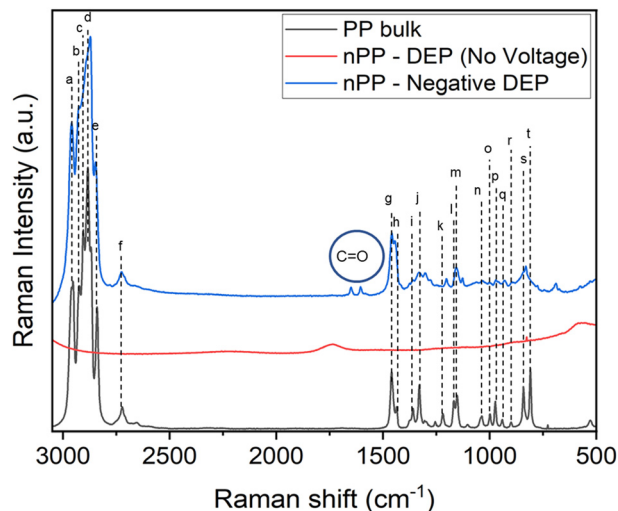


Fig. 7 Raman spectra (from bottom to top) of bulk PP, nanoPP with DEP off (background), and nanoPP with DEP on.

an average spectrum. The collected spectra confirmed the material was PP and were in agreement with data obtained by INRiM (see SI, section I for details).

**3.2.4. Polypropylene mass fraction quantification.** The concentration data for nanoPP determined by pyGC-MS are presented in Table 5. Laboratory blanks showed a background ranging from 3–30% of the PP, which was not subtracted from the reported concentrations. The calculated concentration depended on the selected markers. This was due to the discrepancy in relative peak response of the individual peaks in the duplet and triplet compounds between the PP reference material used to construct calibration curves and the nanoPP. The racemic 2,4,6-trimethyl-1-nonene and heterotactic 2,4,6,8-tetramethyl-1-undecene peaks were significantly higher in relative abundance in the nanoPP compared to the PP reference material (and to what is commonly observed in isotactic PP). The data generated using these markers are therefore likely to overestimate the nanoPP concentration in the samples. The concentration of nanoPP would then be in the range 3–5  $\mu\text{g mL}^{-1}$ , depending on the applied marker.

While it is possible that the nanoPP production process may have caused fragmentation-induced chain scission and oxidation, possibly exacerbated by acetone exposure, the

reference PP powder used for calibration and quantification was also produced *via* a harsh cryo-milling process. It therefore appears most likely that the observed differences in the pyrolysis marker ratios in the pyrograms of the two materials are the result of the differences in the composition of the two different sources of pellets used in their production (SI, section J). These differences in chemical composition between the PP reference material and the nanoPP (produced from a different PP source material) highlight a potential challenge with PP quantification by pyGC-MS. In environmental or human samples, the type of PP present cannot be known and maybe a mixture of different PP particles, meaning the use of a single PP reference material for generating calibration curves could easily over- or underestimate the true PP concentration.

**3.2.5. Determination of inorganic impurities.** Inorganic impurities present in the nanoPP material (detected qualitatively using EDS) were analysed using microwave assisted total ICP-MS. Results of the multielement characterisation showed a variety of elements in the nanoPP suspension, with Si being the most abundant, followed by Al, Mg, K and Ca, which supports elemental mapping obtained with SEM/EDS. Elements detected with ICP-MS were distributed heterogeneously in the sample (as indicated by relatively high stdev of the replicate measurements), potentially due to adsorption of these elements to the surface of the nanoPP particles. Measurements of pristine chemicals (type I reagent grade water, HCl, HNO<sub>3</sub>) and labware (TFM vessels, precleaned PP vessels) did not show significant blank levels of analytes. Si concentrations were exclusively observed in HBF<sub>4</sub>, but at levels at least one order of magnitude lower compared to those in the digests. Hyphenated AF4-ICP-MS was attempted by Postnova to verify if the elements identified were associated with PP particles, but the ICP-MS signal measured in the fractionated peaks was too low to enable on-line quantification. The source of the inorganic contaminants can't be finally clarified but based on the systematic investigation in this study it seems likely to originate from the PP raw material itself.

## 4. Conclusions

The work present here describes the multiparameter physicochemical characterisation of a novel, more

Table 5 Polypropylene mass fraction obtained with pyGC-MS

Marker	nanoPP ( $\mu\text{g mL}^{-1}$ )			Blank ( $\mu\text{g mL}^{-1}$ )		
	Average	Stdev	RSD (%)	Average	Stdev	RSD (%)
Sum 2,4,6-trimethyl-1-nonene	5.0	1.1	22	0.71	0.02	2
Sum 2,4,6,8-tetramethyl-1-undecene	4.3	1.0	24	0.66	0.01	2
2,4-Dimethylhept-1-ene	2.7	0.5	19	0.79	0.01	1
2,4,6-Trimethyl-1-nonene (meso)	3.5	0.7	20	0.75	0.01	1
2,4,6-Trimethyl-1-nonene (race)	9.5	2.1	22	0.73	0.01	1
2,4,6,8-Tetramethyl-1-undecene (iso)	2.8	0.6	23	0.74	0.01	1
2,4,6,8-Tetramethyl-1-undecene (het)	17	4	22	0.5	0.2	30
2,4,6,8-Tetramethyl-1-undecene (syn)	3.7	0.8	22	0.76	0.01	1



environmentally relevant nanoPP test material prepared using a top-down approach employing mechanical fragmentation of PP pellets. The material was characterised for particle size, size distribution, shape, number concentration, polypropylene mass fraction, chemical identity and the content of inorganic impurities using a wide range of analytical methods. The nanoPP material was found to be polydispersed in size, exhibited irregular particle morphologies, and presented signs of oxidative aging. Despite the challenging characteristics of the material, good agreement between the employed techniques was achieved for the key measurands. The increased environmental relevance of the test material means that it has good potential for application in the development and validation of more robust and accurate nanoplastic extraction and quantification methods. Furthermore, the availability of test materials such as the nanoPP produced in this study paves the way for future development and commercialisation of comprehensively characterised nanoPP reference materials that are more representative of critical environmental and food particle-based plastic pollutants of increasing global concern.

## Author contributions

Aneta Sikora: writing – original draft, review and editing, formal analysis, visualisation, investigation, methodology and validation. Dorota Bartczak: conceptualisation, writing – review and editing, supervision, methodology and validation. Heidi Goenaga-Infante: writing – review and editing, supervision. Marta Barbaresi: investigation, formal analysis, writing – review and editing. Francesca Rossi: methodology, investigation, formal analysis. Maurizio Piergiovanni: investigation, writing – review and editing. Monica Mattarozzi: methodology, writing – review and editing. Maria Careri: writing – review and editing, supervision, funding. Andy M. Booth: data validation, writing – review and editing. Lisbet Sørensen: investigation, methodology, formal analysis, writing. Jeremie Parot: methodology, writing – review and editing. Amaia Igartua: investigation, methodology, formal analysis, writing-review and editing. Thierry Caebergs: investigation, methodology, formal analysis, writing – review and editing. Anne-Sophie Piette: investigation, formal analysis. Roland Drexel: investigation, methodology, formal analysis, validation, writing – review and editing. Florian Meier: validation, writing – review and editing, supervision. Francesco Barbero: writing – review and editing, investigation, formal analysis, visualisation, methodology and validation. Ivana Fenoglio: writing – supervision. Charlotte Wouters: methodology, formal analysis, validation, writing, review and editing. Jan Mast: review and editing, supervision. Enrica Alasonati: investigation, methodology, formal analysis, validation, writing – review and editing. Marta Fadda: investigation, formal analysis, writing – review and editing. Alessio Sacco: investigation, formal analysis, writing – review and editing. Andrea Mario Rossi:

supervision, funding. Andrea Mario Giovannozzi: Conceptualisation, writing – review and editing, supervision, methodology, validation and funding.

All authors reviewed and approved the final version of manuscript.

## Conflicts of interest

There are no conflicts to declare.

## Data availability

Supplementary information (SI) is available. See DOI: <https://doi.org/10.1039/d5en00917k>.

## Acknowledgements

The project 21GRD07 PlasticTrace (Funder ID: <https://doi.org/10.13039/100019599>) has received funding from the European Partnership on Metrology, co-financed from the European Union's Horizon Europe Research and Innovation Programme and by the Participating States. METROFOOD-IT project has received funding from the European Union – NextGenerationEU, PNRR—Mission 4 “Education and Research” Component 2: from research to business, Investment 3.1: Fund for the realisation of an integrated system of research and innovation infrastructures—IR0000033 (D.M. Prot. n.120 del 21/06/2022). This publication has been funded by the Italian Ministry of University and Research (MUR) in the framework of the continuing-nature project “NEXT-GENERATION METROLOGY”, under the allocation of the Ordinary Fund for research institutions (FOE) 2023 (Ministry Decree n. 789/2023). Research and innovation network on food and nutrition Sustainability, Safety and Security—Working ON Foods” (ONFOODS) project which received funding from the NRRP and the Mission 4 Component 2 Investment 1.3-Call for tender No. 341 of 15/03/2022 of the Italian Ministry of University and Research funded by the European Union—NextGenerationEU. Award Number: Project code PE0000003.

## References

- 1 H. Ritchie, How much plastic waste ends up in the ocean? OurWorldinData.org, 2018, last accessed 18/09/25.
- 2 EU (2020) Directive 2020/2184 of the European Parliament and of the Council of 16 December 2020 on the quality of water intended for human consumption (recast). Official J EU 23.12.2020.435.
- 3 P. N. T. Pilapitiya and A. S. Ratnayake, The world of plastic waste: A review, *Cleaner Mater.*, 2024, **11**, 100220.
- 4 A. L. Andrady, P. W. Barnes, J. F. Bornman, T. Gouin, S. Madronich, C. C. White, R. G. Zepp and M. A. Jansen, Oxidation and fragmentation of plastics in a changing environment; from UV-radiation to biological degradation, *Sci. Total Environ.*, 2024, **851**, 158022.
- 5 ISO/TR 21960:2020 ‘Plastics—environmental aspects—state of knowledge and methodologies’.



- 6 Commission Regulation 2023/2055 of 25 September 2023 amending Annex XVII to Regulation (EC) n. 1907/2006 of the European Parliament and of the Council concerning the Registration, Evaluation, Authorisation and Restriction of Chemicals (REACH) as regards synthetic polymer microparticles, Official Journal of the European Union, 2023.
- 7 J. Gigault, A. Ter Halle, M. Baudrimont, P. Y. Pascal, F. Gauffre, T. L. Phi, H. El Hadri, B. Grassl and S. Reynaud, Current opinion: What is a nanoplastic?, *Environ. Pollut.*, 2018, **235**, 1030–1034.
- 8 M. Wagner, N. B. Hartmann, A. Verschoor, T. Hüffer, M. Hassellöv and R. C. Thompson, Are we speaking the same language? Towards a definition and categorization framework for environmental plastic debris, *Society of Environmental Toxicology and Chemistry, SETAC Europe 28th Annual Meeting*, 2018, 35.
- 9 S. Alqahtani, S. Alqahtani, Q. Saquib and F. Mohiddin, Toxicological impact of microplastics and nanoplastics on humans: understanding the mechanistic aspect of the interaction, *Front. Toxicol.*, 2023, **5**, 1193386.
- 10 R. T. Coones, V. Kestens and C. Minelli, A comparison of hydrodynamic diameter results from MADLS and DLS measurements for nanoparticle reference materials, *J. Nanopart. Res.*, 2025, **27**, 170.
- 11 H. Zhao, X. Wang, R. Wang, D. Hua, K. Li and F. Ji, Optimal static light scattering detection angle for particulate matter size and concentration measurement, *Meas. Sci. Technol.*, 2023, **34**, 125802.
- 12 J. A. Gallego-Urrea, J. Tuoriniemi and M. Hassellöv, Applications of particle-tracking analysis to the determination of size distributions and concentrations of nanoparticles in environmental, biological and food samples, *TrAC, Trends Anal. Chem.*, 2011, **30**, 473.
- 13 C. Wouters, D. Morales, K. Tsilikas, E. Verleysen and J. Mast, A validation methodology for size and shape measurement of nanoplastics by transmission electron microscopy' In BIO Web of Conferences, EDP Sciences, 2024, 129, 26039.
- 14 J. S. Stine, N. Aziere, B. J. Harper and S. L. Harper, A novel approach for identifying nanoplastics by assessing deformation behavior with scanning electron microscopy, *Micromachines*, 2023, **14**, 1903.
- 15 M. Galluzzi, M. Lancia, C. Zheng, V. Re, V. Castelvetro, S. Guo and S. Viaroli, Atomic Force Microscopy (AFM) nanomechanical characterization of micro-and nanoplastics to support environmental investigations in groundwater, *Emerging Contam.*, 2025, **11**, 100478.
- 16 M. J. Huber, N. P. Ivleva, A. M. Booth, I. Beer, I. Bianchi, R. Drexel and O. Geiss, *et al.*, Physicochemical characterization and quantification of nanoplastics: applicability, limitations and complementarity of batch and fractionation methods, *Anal. Bioanal. Chem.*, 2023, **415**, 3007.
- 17 S. Megha, S. Unnimaya, N. Mithun, S. Chidangil, S. Kumar and J. Lukose, *Microplastics in African and Asian Environments: The Influencers, Challenges, and Solutions*, Cham, Springer Nature Switzerland, 2024, p. 647.
- 18 G. Li, Z. Yang, Z. Pei, Y. Li, R. Yang, Y. Liang, Q. Zhang and G. Jiang, Single-particle analysis of micro/nanoplastics by SEM-Raman technique, *Talanta*, 2022, **249**, 123701.
- 19 M. Fadda, A. Sacco and K. Altmann, *et al.*, Tracking nanoplastics in drinking water: a new frontier with the combination of dielectrophoresis and Raman spectroscopy, *Microplast. Nanoplast.*, 2024, **5**, 24.
- 20 A. Placci, M. Fadda, I. Coralli, J. Wang, A. Zattoni, A. L. Costa, R. Portela, A. M. Giovannozzi, D. Fabbri, D. Melucci and S. Giordani, Multitechnique characterization of eco-corona formation on airborne nanoplastics, *RSC Adv.*, 2025, **28**, 30849.
- 21 J. Hildebrandt and A. F. Thünemann, Aqueous dispersions of polypropylene: toward reference materials for characterizing nanoplastics, *Macromol. Rapid Commun.*, 2023, **44**, 2200874.
- 22 J. Mast *et al.*, NANoREG D2.10 SOP 01 Preparation of EM-grids containing a representative sample of a dispersed NM, 2018.
- 23 T. Wagner ParticleSizer, <https://zenodo.org/badge/latestdoi/10.1111/18649/thorstenwagner/ij-particlesizer>, last accessed on 18/09/2025.
- 24 E. Verleysen, T. Wagner, H. G. Lipinski, R. Kägi, R. Koeber, A. Boix-Sanfeliciu, P. J. De Temmerman and J. Mast, Evaluation of a TEM based Approach for Size Measurement of Particulate (Nano) materials, *Materials*, 2019, **12**, 2274.
- 25 M. Piergiovanni, M. Mattarozzi, E. Verleysen, L. Siciliani, M. Suman, F. Bianchi, J. Mast and M. Careri, The Combined ICP-MS, ESEM-EDX, and HAADF-STEM-EDX Approach for the Assessment of Metal Sub-Micro- and Nanoparticles in Wheat Grain, *Molecules*, 2024, **29**, 3148.
- 26 N. Riboni, E. Ribezzi, L. Nasi, M. Mattarozzi, M. Piergiovanni, M. Masino, F. Bianchi and M. Careri, Characterization of Small Micro-and Nanoparticles in Antarctic Snow by Electron Microscopy and Raman Micro-Spectroscopy, *Appl. Sci.*, 2024, **14**, 1597.
- 27 J. Foucher, A. Labrosse, A. Dervill'e, Y. Zimmermann, G. Bernard, S. Martinez, H. Grönqvist, J. Baderot and F. Pinzan 'The Coming of Age of the First Hybrid Metrology Software Platform Dedicated to Nanotechnologies (Conference Presentation)' <https://www.spiedigitallibrary.org/conference-proceedings-of-spie/10145/1014507/The-coming-of-age-of-the-first-hybrid-metrology-software/> DOI: [10.1117/12.2258093.short?SSO=1](https://doi.org/10.1117/12.2258093.short?SSO=1), last accessed 18/09/25.
- 28 N. Bouzakher-Ghomrasni, O. Taché, J. Leroy, N. Feltin, F. Testard and C. Chivas-Joly, Dimensional measurement of TiO<sub>2</sub> (Nano) particles by SAXS and SEM in powder form, *Talanta*, 2021, **234**, 122619.
- 29 ISO/TS 21362:2018 'Nanotechnologies-Analysis of nano-Objects using asymmetrical-flow and centrifugal field flow fractionation'.
- 30 S. Bouhellal, PCT/DZ02/00001, WO 02/085973 A1, 2002, <https://patentimages.storage.googleapis.com/95/a4/96/b3961c6f59549d/WO2002085973A1.pdf>, last accessed 18/09/2025.
- 31 K. Altmann, L. Wimmer, V. Alcolea-Rodriguez, T. Waniek, V. Wachtendorf, K. Matzdorf, D. Ciornii, P. Fengler, F. Milczewski, I. Otazo-Aseguinolaza and M. Ferrer, Quality-by-design and current good practices for the production of test and reference materials for micro-and nano-plastic research, *J. Hazard. Mater.*, 2025, **18**, 139595.



- 32 K. Altmann, R. Portela, F. Barbero, E. Breuninger, L. M. Camassa, T. C. Velickovic, C. Charitidis, A. Costa, M. Fadda, P. Fengler and I. Fenoglio, Characterizing nanoplastic suspensions of increasing complexity: inter-laboratory comparison of size measurements using dynamic light scattering, *Environ. Sci.: Nano*, 2025, **12**, 5242.
- 33 M. Glais, T. Falher, E. Deniau, C. Chassenieux and F. Lagarde, Elaborating more realistic model microplastics by simulating polypropylene's environmental ageing, *Ecotoxicol. Environ. Saf.*, 2024, **283**, 116769.
- 34 S. Lambert and M. Wagner, Formation of microscopic particles during the degradation of different polymers, *Chemosphere*, 2016, **161**, 510.

